Hilder *et al.* (2009) stated that BNNT showed superior in water flow properties and 100 % of salt rejection theoretically. In the same experiment, they stated that increasing in the radius of the BNNT would shift the tube become ions selective from cations to anions. In comparison, BN is expected to be more efficient in purifying water than CNT. There is a need to further explore the potential of utilizing newly emerging BN nanoparticles in membrane desalination application. The science behind the performance improvement needs to be elucidated.

The objective of this study was to identify the performance of various type of BN in desalination. A series of characterization were conducted to understand the physical and chemical properties of various types of BN and their effects on the membrane performance. The new type of TFN membrane was determined through the membrane surface hydrophilicity and structural properties as well. Performances of the membrane were further evaluated through salt rejection and pure water permeability.

EXPERIMENTAL

Materials

All chemicals were used as received without further modification. Polysulfone Udel ® P-3500 in pellet form (Solvay), 1-methyl-2-pyrrolidinone (NMP, 99 %, Acros Organics) and polyethylene glycol 400 (PEG 400) were used for fabrication of PSf substrate. Trimesoyl chloride (TMC, 98 %, Acros Organics) and m-phenylenediamine (MPD, 99 %, Merck) were used as the monomers to sculpt the PA layer on PSf substrate via interfacial polymerization. n-Hexane (99 %) from RCI Labscan was used as solvent for TMC. Boron nitride powder (<1 μm, Sigma Aldrich) was used as membrane filler for this study. Sodium chloride (NaCl, Merck) was used as solute to determine the performance of membrane in salt rejection.

Chemical activation of BN

BN activation was carried out by adding 3 g of h-BN into 50 w/w % of the activating reagent which is the mixture of 1 M H_2SO_4 aqueous solution and 8 M HNO3 aqueous solution with a weight ratio of 1:1. The mixture underwent ultrasonication for 30 min at room temperature. The activation procedure end up by stirred the obtained slurry mechanically in an 80 °C water bath for another 2 hours. After activation process, the sample was washed with deionized water until the pH of the rinse in the neutral range (pH 6.8-7.2). To remove the moisture presented, the prepared sample was dried in oven at 105 °C for 24 hours and labeled as activated BN (A-BN) (Li *et al.*, 2015).

Preparation of PSf and PSf/BN substrates

PSf substrates were prepared according to the dope formulation as shown in Table 1. To prepare the PSf/BN membrane, an appropriate amount of PEG and BN / A-BN were added to the NMP solution. The mixture was then undergoes ultrasonification for 30 min to avoid the agglomeration of BN. After that, PSf was slowly added into the mixture under vigorous stirring to produce the casting solution. The solution was then undergoes ultrasonication for another 1 hour to remove the air bubbles trapped within the solution. The PSf substrate was cast on the glass plate by using glass rod. To allow phase immersion process occurred, the cast membrane was immersed into water coagulation bath immediately. After membrane had been peeled off from the glass plate, the membrane was transferred into another water bath for at least 24 hours before used.

Table 1 Dope formulation of the casting solutions.

Membrane	Dope Formulation (wt %)			
	PSf	PEG 400	Nanoparticles	NMP
TFC	15	2	0	83.0
TFN-1	15	2	0.5 BN	82.5
TFN-2	15	2	0.5 A-BN	82.5
TFN-3	15	2	0.5 BN	82.5
TFN-4	15	2	0.5 A-BN	82.5

Preparation of TFC/TFN membranes

Polyamide selective layer was formed on the as prepared mixed matrix membrane via interfacial polymerization between MPD and TMC. Firstly, the substrate was clamped in between a glass plate and Viton frame. 30 ml of 2 w/v% MPD solution was poured into the frame and allowed to contact with the porous PSf for 2 min before those excess MPD solution drained off. A rubber roller was used to remove those residual droplets from the substrates by rolling across the surface of membrane. 20 ml of 0.2 w/v% of TMC in hexane solution was then poured into the frame with 1 min contact time with the substrate surface. Both BN and A-BN was added into the TMC solution and poured onto PSf/BN and PSf/A-BN substrates. A thin active PA layer was formed immediately resulted from the interaction of MPD and TMC monomers. Those excess organic solutions were drained off. The membrane was then cured in oven for 8 min at 60 °C. The resulting membrane was immersed in DI water until used. These membranes were labeled as TFC, TFN-1 (BN in PSf substrate), TFN-2 (A-BN in PSf substrate), TFN-3 (BN in both PSf substrate and PA layer), TFN-4 (A-BN in both PSf substrate and PA layer) as shown in Table 2.

Table 2 Membranes composition.

Membrane	Composition	
	PSf membrane	PA layer
TFC	PSf	PA layer
TFN-1	0.5 % BN in PSf	PA layer
TFN-2	0.5 % A-BN in PSf	PA layer
TFN-3	0.5 % BN in PSf	0.05 % BN in PA layer
TFN-4	0.5 %A- BN in PSf	0.05 %A- BN in PA layer

BN characterization

The structure of BN particle was examined using transmission electron microscopy (TEM Hitachi HT7700) operated at the transmission mode of 100 kV. Fourier transform infrared spectroscopy (FTIR) of BN was investigated by using spectrum One FTIR Spectrometer (PerkinElmer).

Membrane characterization

Functional groups of BN were investigated using Spectrum One Fourier transform infrared spectroscopy (FTIR) Spectrometer (PerkinElmer) in wavelength that range from 400 to 4000 cm^{-1}. The cross-sectional and the surface morphology of the membrane samples were observed using scanning electron microscopy (SEM, Hitachi TM 3000 Tabletop Microscope). Contact angle (CA) measurement was conducted by sessile drop method employing an automated CA goniometer (OCA 15 pro, DataPhysics) using RO water as probe liquid. Ten measurements were collected at different spots of each membrane sample and the mean value was recorded. Topological properties of the membranes were investigated using atomic force microscopy (Hitachi AFM 5100N). The membrane surface (10μm×10μm) was scanned using non-contact mode. The average roughness (R_a), the root mean square of Z data (R_{ms}) and the mean difference between the highest peak and lowest valleys (R_{max}) were measured.

Membrane filtration performance

A dead-end filtration cell (Sterlitech™ HP4750) was used to assess the permeation of the fabricated substrates and membranes under nitrogen atmosphere. The effective surface area of the membrane was 14.6 cm^2. Prior to any measurement, the membranes were compacted at pressure of 16 bar, respectively for about 30 min to achieve flux steady state condition. The pure water permeability of the substrates was then calculated from the measured permeation flux using pure water at operating pressure of 15 bar. The pure water flux (PWF) of the membranes were operated by using the following equation:

$$J_{WF} = \frac{V}{A\Delta t} \quad (1)$$

where J_{WF} is the water flux (L/m^2h), V is the volume of water permeated across the membrane (L), t is the time taken for collecting the permeate (h) and A_m, is the effective membrane area (cm^2).

Sodium chloride (NaCl) solution of 1000 ppm was tested for reverse osmosis studies. The rejection efficiency, R (%) was calculated based on the following equation:

$$R(\%) = \left(1 - \frac{C_p}{C_f}\right) \times 100 \quad (2)$$

where C_p and C_f are the solute concentration (ppm) in the permeate and feed respectively. All filtration experiments were operated at 15 bar and at room temperature.

RESULTS AND DISCUSSION

BN and A-BN characterizations

The A-BN was characterized in several ways to compare with the commercial BN. Fig. 1 compares the FTIR spectrum of both BN and A-BN. Both BN and A-BN shows two main peaks at ~ 1400 cm^{-1} and 800 cm^{-1} that be in agreement with BN stretching vibrations and B-N-B bending vibrations. There is one new emerging peak that can be observed in A-BN that located at ~ 3250 cm^{-1} indicated the present of B-NH_2 group. Besides, A-BN shows an increment in peak intensity of ~ 1413 cm^{-1} (B-N). This indicated that the A-BN has increase in polarity. Peak broadening in the range of ~830 cm^{-1} to 1550 cm^{-1} also indicated that the size of A-BN decreases and aggregation of nanoparticles (Wang *et al.*, 1998). This can be further confirmed in TEM results.

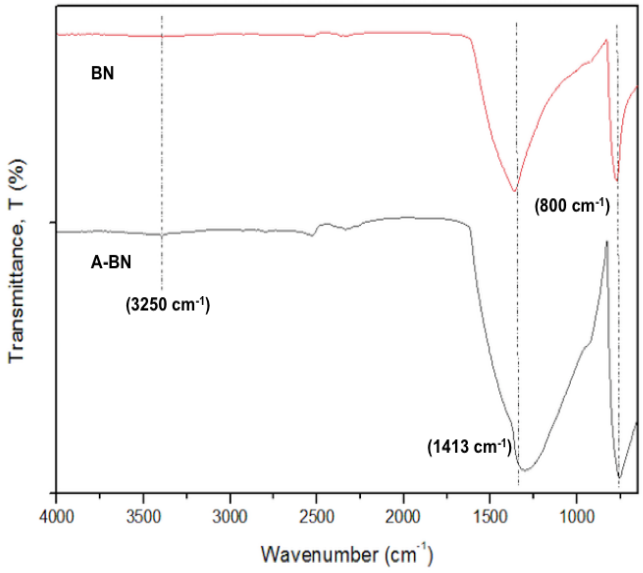

Fig. 1 FTIR spectra of BN and A-BN.

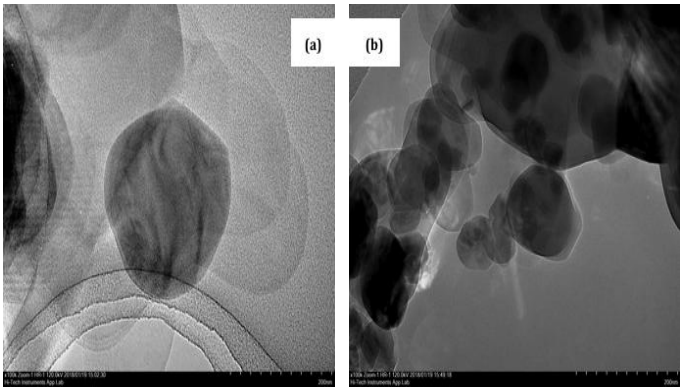

Fig. 2 TEM images of (a) BN and (b) A-BN.

The microstructures of BN and A-BN were investigated by TEM in Fig. 2. Based on the TEM images, the size of the A-BN nanoparticles is smaller than the BN nanoparticles. It is due to the reaction occurs in between BN nanoparticles and concentrated nitric acid, which creates oxidized radicals on BN and form BN-H+ bonds on the surface of BN that might cut and functionalize BN nanoparticles (Ide *et al.*, 2014; Li *et al.*, 2015). This proved that TEM results were in agreement with FTIR results. Besides, the edge of A-BN nanoparticles is found to be rougher as compared to the edge of BN nanoparticles, suggesting that the chemical activation reaction occur on the surface of the A-BN.

Membrane characterizations

Fig. 3 shows the FTIR results of TFC and TFN membranes. Both TFC and TFN membranes show the spectrum at various peaks that corresponding to functional group of the PSf support membranes which, the peaks at the particular wavenumber of 1151 cm^{-1} (symmetric O=S=O stretching), 1242 cm^{-1} (asymmetric C-O-C stretching), 1293 cm^{-1} (asymmetric O=S=O stretching), 1409 cm^{-1} (C=C aromatic ring stretching), and 1503 cm^{-1} (CH3-C-CH3 stretching) (Lau, *et al.*, 2014). The formation of PA layer on TFC and TFN membranes can be confirmed through FTIR results at the peak of 1552 cm-1 and 1585 cm-1 that corresponding to C=O and C-N stretching (Wan Azelee *et al.*, 2017). Moreover, other bands at 1611 cm^{-1} and 1667 cm^{-1} reinforce the formation of PA layer that associated to aromatic amide ring breathing and N-H bending in CO-NH group (Khorshidi *et al.*, 2015). As comparison, the embedment of BN and A-BN into TFN membranes tend to broadening the peak at ~795, ~1325, ~1409 cm^{-1}. This indicated that there is stretching vibration of those functional groups upon the addition of BN and A-BN nanoparticles.

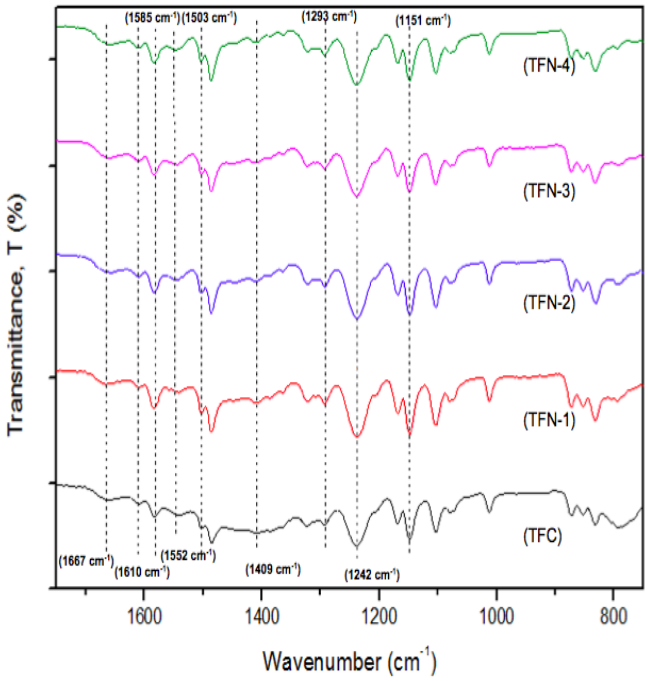

Fig. 3 FTIR of TFC and TFN membranes.

Fig. 4 shows the surface and cross-sectional morphology of the TFC and TFN membranes. The cross-section SEM images of all membranes show that the membranes consist of two layers, which are the PSf support layer and thin-film active layer. All the membranes displayed typically interfacial polymerized characteristic, which consisted of ridge and valley structures. It can be seen clearly in Fig. 4 that those TFN-4 membranes has more ridge and valley structures as compared to other membranes. This observation further confirms the AFM images. Both BN and A-BN were dispersed nicely in both PSf support layer and PA active layer since there is no agglomeration observed in the SEM images.

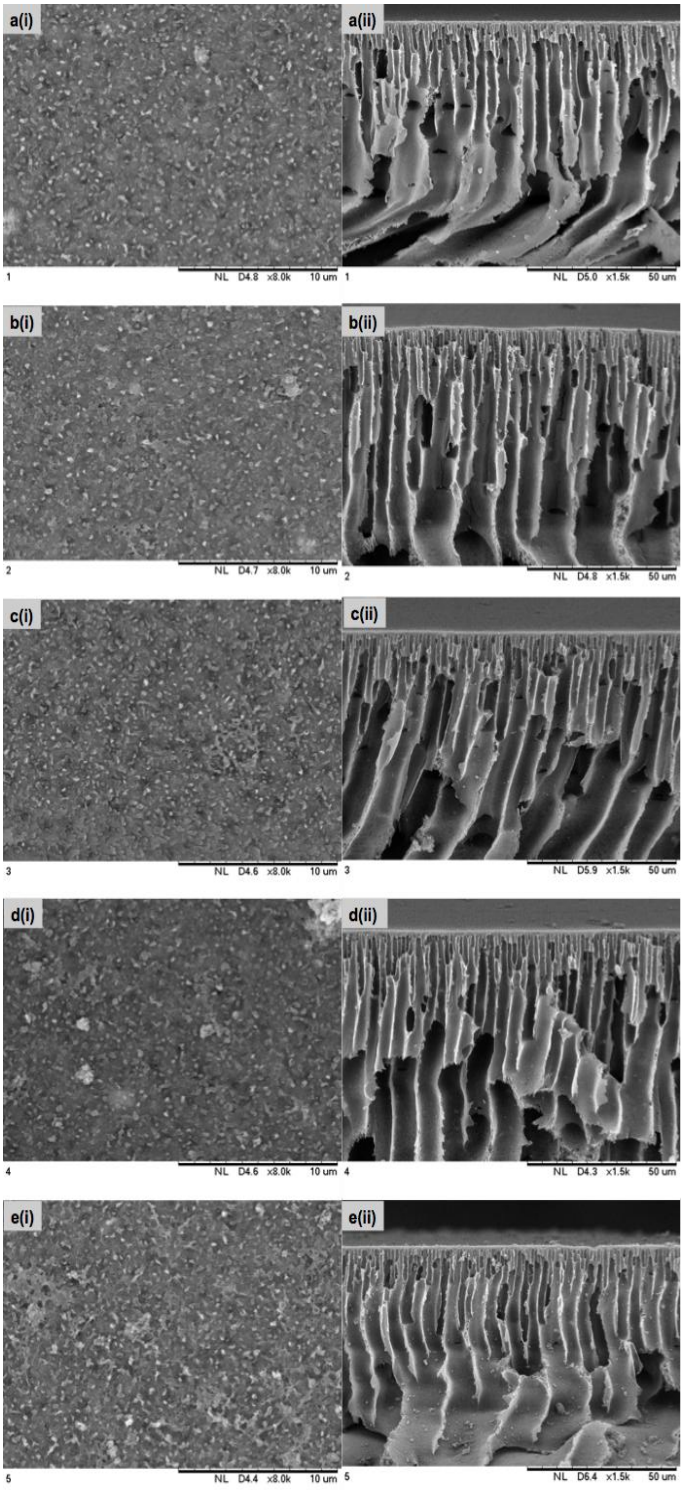

Fig. 4 SEM images for (a) TFC, (b) TFN-1, (c) TFN-2, (d) TFN-3, (e) TFN-4 membranes (i: surface; ii: cross-sectional morphology).

Fig. 5 shows the 3D AFM images of the top surface of TFC and TFN membrane upon addition of BN and A-BN into the PSf substrate and PA surface of membrane. As seen from Fig. 4, both TFC and TFN membranes have ridge and valley structure. The embedment of BN and A-BN into TFN membranes exhibited significant rougher surface compared to TFC membrane. The increase in surface roughness could be due to the enlargement of effective surface area. The increase in surface roughness can be advantageous for water permeability since its provide a higher surface area for water molecules to flow through (Lai *et al.*, 2016). Further surface roughness parameters show in Table 3. R_{ms} values of TFN membranes show distinct increment with the maximum Rms value (113.7 nm) found in TFN-4. From Fig. 5, the embedment of A-BN into TFN-4 has created a higher ridges which indicated increasing in surface roughness of membrane.

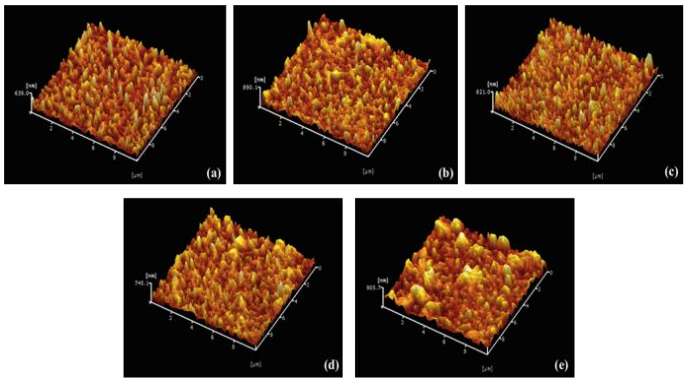

Fig. 5 AFM images for (a) TFC, (b) TFN-1, (c) TFN-2, (d) TFN-3, (e) TFN-4.

Table 3 Surface roughness of TFC and TFN membranes.

Membrane	Surface roughness parameter (nm)		
	Ra	Rms	Rmax
TFC	54.01	70.47	525.6
TFN-1	67.3	85.55	569.1
TFN-2	71.4	93	701.6
TFN-3	64.74	84.48	681.4
TFN-4	90.38	113.7	722.8

Table 4 shows the surface contact angle of TFC and TFN membranes. It is reported that embedment of BN and A-BN into TFN membranes tended to decrease the contact angle. The contact angle decreased from 78.85 to 69.92° for TFN-4. The reduction in contact angle is due to the activation process of BN that facilitate the functional group, B-NH_2 into BN nanosheets. The existence of B-NH_2 group as polar functional group provides the A-BN hydrophilic behavior by forming hydrogen bonding in between B-NH_2 and water molecules.

Table 4 Contact angle of TFC and TFN membranes.

Membrane	Contact angle (°)
TFC	78.85 ± 4.32
TFN-1	75.38 ± 4.91
TFN-2	75.18 ± 5.16
TFN-3	72.77 ± 3.91
TFN-4	69.92 ± 4.74

Fig. 6 shows the effect of BN on PWP performance and NaCl rejection of TFC and TFN membranes. The TFN membranes that incorporated with BN and A-BN nanoparticles exhibited better performance in water flux property than TFC. In comparison, embedment of A-BN nanoparticles into both PSf substrates and PA layer of TFN showed higher PWP than the TFN membrane that containing pristine BN. TFN-4 exhibited the best water permeability among the membrane with 1.16 L/m^2 h bar, which was approximately 33.9 % higher than TFC membrane. The improvement in PWP TFN-4 membrane was due to the decreasing in surface contact angle and increasing in surface roughness of membrane. The present of NH_2 group in BN aid in increase the hydrophilicity of BN by forming hydrogen bonding with water and allowed water molecule take precedence to flow through (Zhong *et al.*, 2015). The incorporation of nanoparticles into the TFN membranes does not aid in increasing the rejection capability of membranes. TFC control membrane possessed the highest NaCl rejection among the membrane with ~95 %. With the embedment of BN and A-BN as nanofillers into both PSf substrate and PA layer, the NaCl rejection of TFN membranes slightly decreases. The NaCl rejection for TFN-1 and TFN-2 was 87 % and 93 %, respectively. While for TFN-3 and TFN-4, the NaCl rejection was decreased to 81 % and 89.84 %, respectively. The decrease in NaCl rejection might due to lack of functional group on BN and A-BN. The chemically activated BN possess B-NH_2 that can aid in increase water permeability of TFN membranes. Li *et al.* (2015) had conducted the activation process on BN fibers and the results obtained was slightly differ from this

experiment. In comparison, the chemical activation BN fiber possesses B-OH group and a more obvious B-NH_2 group. Meanwhile, the chemical activation method proposed by Li *et al.* was unsuitable to be used on BN (hexagonal shape) due to the properties of BN, which thermal and chemically inertless (Falin *et al.*, 2017). In overall, TFN membranes that incorporated with A-BN nanoparticles show better overall performances as PWF take into consideration.

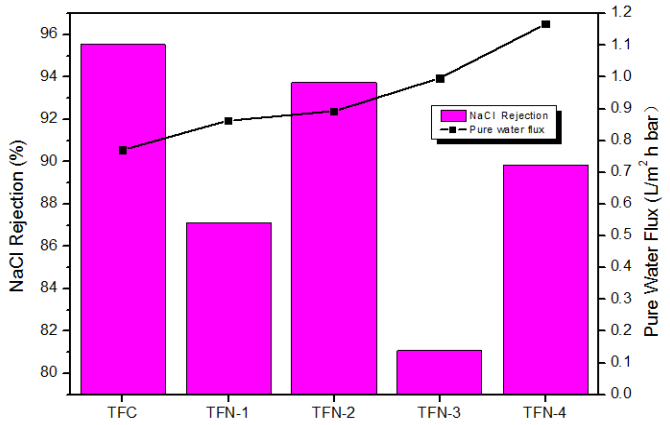

Fig. 6 Pure water flux and NaCl rejection of TFC and TFN membranes.

CONCLUSION

In this experiment, A-BN that was undergoes chemical activation process and incorporated into PSf and PA layer of TFN membranes. The obtained TFN membranes showed improvement in water permeability with a slightly decrease in NaCl rejection capability. Further investigation was needed to identify the chemical activation process on BN. However, BN nanomaterial has the potential to be used as nanofillers in water purification application if the functional group attached can be specifically tailored.

ACKNOWLEDGEMENT

The authors are grateful for the research grant provided by Ministry of Education (MoE) Malaysia, HiCoE Research grant (R.J090301.7846.4J200) and Fundamental Research Grant Scheme (FRGS) (R.J130000.7846.4F981) for providing financial assistance in this project.

REFERENCES

Sheikholeslami, R. 2009. Strategies for future research and development in desalination challenges ahead. *Desalination*, *248*(1-3), 218-224.

Choi, W., Jeon, S., Kwon, S. J., Park, H., Park, Y., Nam, S., Lee, P. S., Lee, J. S., Choi, J., Hong, S., Chan, E. P., Lee, J. H. 2017. Thin film composite reverse osmosis membranes prepared via layered interfacial polymerization. *Journal of Membrane Science*, *527*, 121-128.

Cadotte, J. E., Petersen, R. J., Larson, R. E., Erickson, E. E. 1980. A new thin-film composite seawater reverse osmosis membrane. *Desalination*, *32*, 25-31.

Lau, W. J., Ismail, A. F., Misdan, N., Kassim, M. A. 2012. A recent progress in thin film composite membrane: A review. *Desalination*, *287*, 190-199.

Goh, P. S., Ismail, A. F., Ng, B. C. 2013. Carbon nanotubes for desalination: performance evaluation and current hurdles. *Desalination*, 308, 2-14.

Goh, P. S., Ismail, A. F. 2015. Graphene-based nanomaterial: The-state-of-the-art material for cutting edge desalination technology. *Desalination*, *356*, 115-128.

Lai, G. S., Lau, W. J., Goh, P. S., Ismail, A. F., Yusof, N., Tan, Y. H. 2016. Graphene oxide incorporated thin film nanocomposite nanofiltration membrane for enhanced salt removal performance. *Desalination*, 387, 14-24.

Das, R., Ali, M. E., Hamid, S. B. A., Ramakrishna, S. Chowdhury, Z. Z. 2014. Carbon nanotube membranes for water purification: A bright future in water desalination. *Desalination*, 336, 97-109.

Goldberg, D., Bando, Y., Huang, Y., Terao, T., Mitome, M., Tang, C. 2010. Boron nitride nanotubes and nanosheets. *American Chemical Society*, *4*(6), 2979-2993.

Hilder, T. A., Gordon, D., Chung, S. H. 2009. Salt rejection and water transport through boron nitride nanotubes. *Small Journal*, *5*(19), 2183-2190.

Li, J., Huang, Y., Liu, Z., Zhang, J., Liu, X., Luo, H., Ma, Y., Xu, X., Lu, Y., Lin, J., Zou, J. 2015. Chemical activation of boron nitride fibers for improved cationic dye removal performance. *Journal of Materials Chemistry A*, *3*(15), 8195-8193.

Wang, Y., Muramatsu, A., Sugimoto, T. 1998. FTIR analysis of well-defined α-Fe2O3 particles. *Colloids and Surfaces A: Physicochemical and Engineering Aspects*, *134*(3), 281-297.

Ide, Y., Liu, F., Zhang, J., Kawamoto, N., Komaguchi, K., Bando, Y., Golberg, D. 2014. Hybridization of Au nanoparticle loaded TiO_2 with BN nanosheets for efficient solar-driven photocatalysis. *Journal of Material Chemistry A*, *2*(12), 4150-4156.

Lau, W. J., Ismail, A. F., Goh, P. S., Hilal, N., Ooi, B. S. 2014. Characterization methods of thin film composite nanofiltration membranes. *Separation & Purification*, *44*(2), 135-156.

Wan Azelee, I., Goh, P. S., Lau, W. J., Ismail, A. F., Rezaei-DashtArzhandi, M., Wong, K. C., Subramaniam, M. N. 2017. Enhanced desalination of polyamide thin film nanocomposite incorporated with acid treated multiwalled carbon nanotube-titania nanotube hybrid. *Desalination*, *409*, 163-170.

Khorshidi, B., Thundat, T., Fleck, B. A., Sadrzadeh, M. 2015. Thin film composite polyamide membranes: parameric study on the influence of synthesis conditions. *Royal Society of Chemistry*, *5*(68), 54985-54997.

Zhong, J., Zhao, Y., Li, L., Francisco, J. S., Zheng, X. C. 2015. Interaction of NH_2 radical with the surface of a water droplet. *Journal of The American Chemical Society*, *137*(37), 12070-12078.

Falin, A., Cai, Q., Santos, E. J. G., Scullion, D., Qian, D., Zhang, R., Yang Z., Huang, S., Watanabe, K., Taniguchi, T., Barnett, M. R., Chen, Y., Ruoff, R. S., Li, L. H. 2017. Mechanical properties of atomically thin boron nitride and the role of interlayer interactions. *Nature Communications*, 15815.